

REPORT DOCUMENTATION PAGE

AFRL-SR-AR-TR-05-

Public reporting burden for this collection of information is estimated to average 1 hour per response, including the time for reviewing instructions, searching existing data sources, gathering the data needed, and completing and reviewing this collection of information. Send comments regarding this burden estimate or any other aspect of this collection of information, including suggestions for reducing this burden to Washington Headquarters Services, Directorate for Information Operations and Reports (0704-0188). Respondents should be aware that notwithstanding any other provision of law, no person shall be subject to any penalty for failing to provide information unless it is required by law. PLEASE DO NOT RETURN YOUR FORM TO THE ABOVE ADDRESS.

1 the
ing
2-
ently

0519

1. REPORT DATE (DD-MM-YYYY) 01 Sep 2005		2. REPORT TYPE Final		PERIOD COVERED (From - To) 01 Sep 2004 to 31 May 2005	
4. TITLE AND SUBTITLE Neural Network Based Adaptive Flow Control for Maneuvering Vehicles				5a. CONTRACT NUMBER FA9550-04-C-0075	
				5b. GRANT NUMBER	
				5c. PROGRAM ELEMENT NUMBER	
				5d. PROJECT NUMBER	
				5e. TASK NUMBER	
6. AUTHOR(S) J. Eric Corban - Guided Systems Technologies, Inc. An Glezer - Georgia Institute of Technology Anthony Calise - Georgia Institute of Technology				5f. WORK UNIT NUMBER	
				8. PERFORMING ORGANIZATION REPORT NUMBER GST-FA9550-03	
				10. SPONSOR/MONITOR'S ACRONYM(S)	
7. PERFORMING ORGANIZATION NAME(S) AND ADDRESS(ES) Guided Systems Technologies, Inc. P.O. Box 1453 McDonough, Georgia 30253-1453				11. SPONSOR/MONITOR'S REPORT NUMBER(S)	
				9. SPONSORING / MONITORING AGENCY NAME(S) AND ADDRESS(ES) AFOSR 875 North Randolph St. Suite 325, Room 3112 Arlington, Virginia 22203	
12. DISTRIBUTION / AVAILABILITY STATEMENT <p style="text-align: center; font-size: 1.2em;">Approved for public release, distribution unlimited</p>					
13. SUPPLEMENTARY NOTES					
14. ABSTRACT This report documents a phase I STIR effort with the objective of developing and demonstrating effective nonlinear adaptive control of the aerodynamic flow about a dynamic body using a distributed array of synthetic jets for actuation. Design of a wind-tunnel test apparatus is presented. Motion of the model is constrained to two degrees of freedom. A conventional elevator is used to trim the model and change its dynamic characteristics. Position control of the model is achieved by an adaptive outer loop controller. This outer loop commands the flow control actuators. A dynamic simulation model of the wind tunnel apparatus is presented, as are designs for both the inner and outer loop controllers. The outer loop design is adaptive. A non-minimum phase transfer function is presented to model the active flow control actuators, and includes possible coupling effects between actuation, the dynamics of flow field, and the rigid body dynamics of the model. The outcomes of simulation studies are presented. The parameters were selected to have an adverse effect on the closed loop response, therefore representing a hypothetical worst-case situation. These results demonstrate successful adaptive control of the simulated wind tunnel test article employing flow devices for actuation.					
15. SUBJECT TERMS Design of Wind Tunnel Test Apparatus. Modeling, Simulation and Control of Test Article. Simulation Results.					
16. SECURITY CLASSIFICATION OF: Unclassified			17. LIMITATION OF ABSTRACT UL	18. NUMBER OF PAGES 28	19a. NAME OF RESPONSIBLE PERSON J. Eric Corban
a. REPORT Unclassified	b. ABSTRACT Unclassified	c. THIS PAGE Unclassified			19b. TELEPHONE NUMBER (include area code) 770-898-9100

20060103 102

AIR FORCE OFFICE OF SCIENTIFIC RESEARCH

01 DEC 2005

Page 1 of 1

DTIC Data

Purchase Request Number: FQ8671-0401283

BPN:

Proposal Number: 04-NM-166

Type Submission: New Work Effort

Inst. Control Number: FA9550-04-C-0075DEF

Institution: GUIDED SYSTEMS TECHNOLOGIES INC

Primary Investigator: Dr. J. Eric Corban

Invention Ind: none

Project/Task: STTRT / X

Program Manager: Sharon A. Heise

Objective:

The purpose of this effort is to demonstrate adaptive output feedback for control of synthetic jets to produce desired control moments on an aerodynamic surface without requiring detailed models of local flow phenomena.

Approach:

In phase I of this program, a dynamic model of a 2-dimensional airfoil equipped with synthetic jet actuators will be produced, and adaptive closed-loop control of airfoil attitude will be demonstrated in simulation. Phase II will provide a real-time wind-tunnel demonstration of this adaptive closed-loop flow control technology for a 3-dimensional aerodynamic configuration that both rotates and translates at various low-speed conditions.

Progress:

Year: 2005 **Month:** 05 **Final**

Final Report For FA9550-04-C-0075

This report documents a phase I STTR effort with the objective of developing and demonstrating effective nonlinear adaptive control of the aerodynamic flow about a dynamic body using a distributed array of synthetic jets for actuation. Design of a wind-tunnel test apparatus is presented. Motion of the model is constrained to two degrees of freedom. A conventional elevator is used to trim the model and change its dynamic characteristics. Position control of the model is achieved by an adaptive outer loop controller. This outer loop commands the flow control actuators. A dynamic simulation model of the wind tunnel apparatus is presented, as are designs for both the inner and outer loop controllers. The outer loop design is adaptive. A non-minimum phase transfer function is presented to model the active flow control actuators, and includes possible coupling effects between actuation, the dynamics of flow field, and the rigid body dynamics of the model. The outcome of simulation studies are presented. The parameters were selected to have an adverse effect on the closed loop response, therefore representing a hypothetical worst-case situation. These results demonstrate successful adaptive control of the simulated wind tunnel test article employing flow devices for actuation. Adaptation to both unmodeled unsteady aerodynamic effects, and changes in angle of attack and airspeed are demonstrated, clearly establishing feasibility. Alternate flow control actuation schemes were also developed in phase 1, highlighting a key advantage of the nonlinear adaptive control approach - that it can be applied to a variety of flow control devices, not just synthetic jets, and to any combination thereof. A phase II program is recommended in which the developed test apparatus and controller are evaluated in the wind tunnel and then demonstrated in free flight.

Neural Network Based Adaptive Flow Control for Maneuvering Vehicles

Phase I Final Report September 2005

Reporting Period: 9/1/04 – 5/31/05

STTR Phase I
Contract FA9550-04-C-0075

Prepared for:

Air Force Office of Scientific Research
ATTN: Lt Col Sharon Heise - NM
875 North Randolph Street
Suite 325, Room 3112
Arlington, Virginia 22203
703-696-7796

By:

J. Eric Corban, Guided Systems Technologies, Inc.
Ari Glezer and Anthony Calise, Georgia Institute of Technology

Guided Systems Technologies, Inc.

P.O. Box 1453
McDonough, Georgia 30253-1453
(770) 898-9100

Abstract

This report documents a phase I STTR effort with the objective of developing and demonstrating effective nonlinear adaptive control of the aerodynamic flow about a dynamic body using a distributed array of synthetic jets for actuation. Design of a wind-tunnel test apparatus is presented. Motion of the model is constrained to two degrees of freedom. A conventional elevator is used to trim the model and change its dynamic characteristics. Position control of the model is achieved by an adaptive outer loop controller. This outer loop commands the flow control actuators. A dynamic simulation model of the wind tunnel apparatus is presented, as are designs for both the inner and outer loop controllers. The outer loop design is adaptive. A non-minimum phase transfer function is presented to model the active flow control actuators, and includes possible coupling effects between actuation, the dynamics of flow field, and the rigid body dynamics of the model. The outcome of simulation studies are presented. The parameters were selected to have an adverse effect on the closed loop response, therefore representing a hypothetical worst-case situation. These results demonstrate successful adaptive control of the simulated wind tunnel test article employing flow devices for actuation. Adaptation to both unmodeled unsteady aerodynamic effects, and changes in angle of attack and airspeed are demonstrated, clearly establishing feasibility. Alternate flow control actuation schemes were also developed in phase I, highlighting a key advantage of the nonlinear adaptive control approach - that it can be applied to a variety of flow control devices, not just synthetic jets, and to any combination thereof. A phase II program is recommended in which the developed test apparatus and controller are evaluated in the wind tunnel and then demonstrated in free flight.

Acknowledgements

The authors would like to acknowledge the outstanding contributions to this work made by John Ripley Culp in the design of the test apparatus, and by Ali Turker Kutay in the modeling, development and analysis of the control system. Both served the program while employed as researchers at the Georgia Institute of Technology.

Table of Contents

1.	Background	1
2.	Design of Wind Tunnel and Free Flight Test Apparatus	4
2.1	Overview.....	4
2.2	Wind Tunnel Model Design Elements	4
2.3	Flow Control Approach	7
3.	Modeling, Simulation and Control of Test Article	10
3.1	Abstract.....	10
3.2	Nomenclature.....	10
3.3	Introduction.....	11
3.4	Passive Traverse Design and Equations of Motion	12
	Aerodynamic Forces	12
	Linearization	14
	Trimming.....	14
3.5	Controller Design.....	16
	Trim Controller Design	16
	Inner Loop Controller Design	17
	Outer Loop Controller Design	17
	Linear Compensator Design for the Outer Loop.....	18
	Error Dynamics	18
	Adaptive Neural Network Design for the Outer Loop.....	19
	Control Hedging.....	19
3.6	Actuator Modeling.....	19
	Elevator Model.....	20
	Active Flow Control Actuator Model	20
3.7	Simulation Results	21
4.	Summary, Conclusions, Recommendations.....	25
	References	27
	Appendix A: Design of an Alternate Test Apparatus	28

1. Background

This is the final report for STTR Phase I Contract FA9550-04-C-0075.

The original program solicitation, AF04-T027, provides the overall program objective: "Demonstrate effective nonlinear adaptive control of the aerodynamic flow about a dynamic body using a distributed array of synthetic jets for actuation." As detailed in our program proposal, we (GST and Georgia Tech) refined our current approach to adaptive output feedback control, and applied it to the problem of active synthetic jet control to maneuver an aircraft. Key phase I objectives, reproduced from the phase I proposal, were:

- Develop a simple dynamic model of a 2-D airfoil with synthetic jet actuator using existing data. The airfoil shall be free to pivot in the pitch axis and shall be balanced using a servo-motor.
- Evolve a neural network (NN) based adaptive feedback method for control of wing attitude using synthetic jet actuation at varying low speed flight conditions. *The control system design shall minimize dependence on an exact model of, or detailed measurement of, local flow phenomenon.*
- Demonstrate effective control of the pivoted wing's attitude using the methods developed under Objective 3 in numerical simulation at varying low speed conditions.
- Design a test apparatus representative of the 2-D airfoil section with pivot identified under Objective 2. The design for the test article shall be derived from existing Georgia Tech designs, and will be suitable for testing in an existing Georgia Tech low-speed wind tunnel facility. The proposed design will include jet actuator arrays that will be suitable for transient actuation to exploit flow nonlinearities. MEMS-based actuators and sensors will be considered.
- Refine the dynamic model of Objective 2, and evaluate the controller of Objective 3 in simulation based on the refined model. Completion of this objective shall clearly demonstrate the feasibility and merit of the proposed closed-loop flow control technology.
- Complete the conceptual design of a phase II test article to fully demonstrate dynamic closed-loop attitude control of a 3-D aerodynamic configuration that both rotates and translates over a range of flight conditions using arrays of synthetic jets for actuation.

Synthetic jet devices have been the subject of extensive research by team members for many years, and are known to be useful for a variety of flow control applications. The effects of these devices are typically demonstrated by wind tunnel testing of 2-D airfoils that are fixed in relation to the airflow. The jets are open-loop driven by using amplitude and frequency modulated waveforms that are experimentally derived. Both the modulation amplitudes and frequencies are highly dependent on dynamic pressure and other factors. It is expected that practical implementation on free-flight vehicles will either require the development of high fidelity physics-based models of the local flow phenomenon during transient conditions from

which a feedback controller can be designed, or require the development of a nonlinear adaptive control approach that largely eliminates design dependence on a model. Suitable physics-based models of the influence of synthetic jets on local flow phenomenon under dynamic conditions are not known to exist. AFOSR has recently selected a MURI proposal from team members to perform the basic research that must first be completed to pursue a model-based control approach. The ultimate control design will likely exploit both approximate physics-based models *and* adaptive control, with feedback of both inertially sensed variables such as attitude and attitude rates, and local sensed flow states such as pressure.

This STTR, with the objective of near-term practical application of leap-ahead technology, was focused on use of nonlinear adaptive control to minimize dependence on modeling and measurement of local flow phenomenon. GST and Georgia Tech have previously demonstrated the ability to largely eliminate dependence on aerodynamic modeling in the design of flight control systems for a variety of platforms in USAF funded programs using nonlinear NN based adaptive control. Theoretical development has been centered at Georgia Tech and supported by AFOSR for a number of years, with Prof. Calise as the principle investigator. Most recently, techniques pioneered on precision guided munitions by a GST-led team under an Air Force SBIR have been employed to demonstrate successful guidance to a moving target using a highly modified MK-82 JDAM (a seeker being externally mounted to the nose of the munition) without the benefit of wind tunnel testing of the new configuration. Specifically, NN based adaptive control is employed to overcome in flight the gross parametric uncertainty associated with the new configuration, allowing rapid development and deployment at greatly reduced cost.

The focus of Phase I was to demonstrate successful adaptive control of a simulated wind tunnel test article that employs flow devices for control. This was accomplished in simulation using *only an approximate model of the synthetic jet actuator* derived from experience and existing data, *demonstrating adaptation* to both unmodeled unsteady aerodynamic effects, and changes in angle of attack and airspeed, and *clearly establishing feasibility*. Note that a key advantage of the nonlinear adaptive control approach is that it can be applied to a variety of flow control devices, not just synthetic jets, and to any combination thereof. *Also note that while it is not necessary to employ local flow measurements to implement this approach, it is anticipated that the NN may be able to employ such measurements to advantage.* The experience gained from the simulations during Phase I has also been used for concomitant design of the experimental hardware and wind tunnel model for Phase II of the proposed project. In phase II, the team will further develop the proposed methods, and demonstrate real-time adaptive output feedback control of the dynamics of the test article in the low speed tunnel, with rapid transition at the conclusion of phase II to a free flight demonstration.

Our original plans for the test article, as detailed in progress report for the period 9/1/04 to 2/20/05, were modeled, analyzed, and the outer loop controller design completed. The approach featured an inner loop controller that provided variable model stability, and an outer loop adaptive controller for commanding the pitch attitude and vertical displacement of the model using the flow control actuators. Difficulties in control system design were encountered due to the mass of the proposed test apparatus, and the inertia of the proposed ball screw actuators. Part of the rationale for the heavy traverse mechanism was the long-term need to support instrumentation that can be used to study and characterize the flow phenomenon. About this time in the STTR program, word was received that team members had been selected for the cited MURI award. The availability of the MURI resources to support the development of a test

apparatus appropriate to long term research (directed at developing a better understanding of the flow physics) motivated the team to focus the STTR effort on a unique light weight test article and apparatus. The STTR effort is thus focused on the demonstration of active flow control on a very light weight test article that can be rapidly transformed into a free flight test article near the end of phase II.

Synthetic jet actuation has been designed for the low speed vehicle configuration that will be constructed in phase II. Alternate novel means for low speed flow control, for which the developed control system can be applied equally well, have been devised to illustrate the potential of the proposed control method to enable rapid development of a variety of systems employing many possible flow control devices. One such alternative was detailed in Progress Report 2. GST has identified near-term applications of low-speed active flow control on vehicles from small hand-launched electric powered surveillance aircraft, to high-altitude long endurance sensor craft. Formal collaboration has been initiated with Aerovironment Inc. that will explore these two application areas, and examine the performance benefits in both systems during phase II. For example, the proposed flow control technology, if successful, could be used to eliminate dependence on traditional electro mechanical actuators and moving control surfaces, saving weight and power, and enabling small, extremely simple aircraft efficient enough to maintain flight for many hours by soaring. Alternately, the introduction of large distributed arrays of these simple flow control devices may be used to very efficiently introduce active load alleviation and flutter suppression of a very large low speed flexible wing. The technology may be enabling for extremely efficient long endurance flight (mission duration of a week or more).

2. Design of Wind Tunnel and Free Flight Test Apparatus

2.1 Overview

This chapter is focused on the design of a wind tunnel test apparatus for the proposed Phase II STTR. The original concept involved a wind tunnel model comprised of a nominally 2-D airfoil instrumented with flow control actuators and having two degrees of freedom namely rotation about a spanwise axis through its center of gravity and vertical translation. During design meetings with the STTR Team, it was decided to expand the design to include a light-weight glider-like platform that can be used for autonomous loitering. The mission will use novel, low-power synthetic jet based flow control actuation at the trailing edge of the wing and the tail that will emulate the action of conventional flaps and thereby allow for maneuver without the activation of conventional, servo-powered control surfaces. It is anticipated that this approach will maximize mission duration by reducing the required payload (e.g., batteries and servo hardware).

This report summarizes the various elements of a proposed wind tunnel model having two degrees of freedom (2DF). The proposed model is designed for testing in the Georgia Tech low-speed wind tunnel facility at the Woodruff School of Mechanical Engineering at Georgia Tech. With the tunnel running, the model will be trimmed using servo-actuated control surfaces so that it is effectively "floating" in the middle of the test section with all forces balanced. At that point, the motion of the model will be controlled in pitch and plunge using neural-network-based adaptive flow control. Actuation will be effected by a novel, flow-control approach that is specifically designed for low-speed applications and is based on pairs of adjacent synthetic jet actuators that are mounted at the trailing edge of the aerodynamic surfaces (the wing and the tail) and can be continuously vectored in the downstream direction (i.e., into the wake) to emulate the effect a jet-flap without moving control surfaces. The jet actuators will be fabricated from light-weight (composite) shells that will be integrated into the wing and tail structure and will use piezoelectric drivers as discussed in Section III below. The time-dependent effect of the actuation on the flow will be measured using an array of miniature, integrated high-speed pressure sensors that will be incorporated onto the skin of the lifting surfaces. These sensors will be used as input to the (adaptive) closed-loop flow controller that will also be coupled to a global flight controller for which the translation and angular position of the model within the wind tunnel will be measured optically using laser diode proximity sensors.

2.2 Wind Tunnel Model Design Elements

A global view of the model is shown in Figure 1. The two degrees of freedom model is essentially comprised of a wing and a horizontal stabilizer (a fixed vertical tail may be added later on) that are mounted on a light-weight fuselage rail. The wing has a span of 86 cm and a chord of 15 cm. The span and chord of the horizontal stabilizer are 23 and 10 cm, respectively and the length of the fuselage is 66 cm. The current wing design uses a NACA 4415 airfoil although a number of other airfoils that are normally used for gliders will be considered (e.g., Clark-Y). The model will be constructed from a mix of composites, balsa, and spruce. The aerodynamic surfaces will be covered with heat shrink plastic film. Segments of both the wing

and the tail have servo-controlled movable trailing-edge surfaces (flaps and elevators, respectively). In the present design, the servo mechanisms are located at the nose section of the fuselage and the control rods are not shown for simplicity. The remainder of each trailing edge is instrumented with pairs of synthetic jet actuators as described below. As noted in Section I, the model will be "floated" in the wind tunnel's test section when the tunnel is operated at a prescribed speed by trimming the aerodynamic forces and moments using the servo actuated control surfaces. The model's motion will be guided along a vertical guide rail and its pitch (and angle of attack) will be varied by rotation about a horizontal axle. When the "floating" state is achieved, the conventional control surfaces will be locked and from that instant on, the model's motion *in two degrees of freedom* will be affected in closed loop by using the flow control actuators.

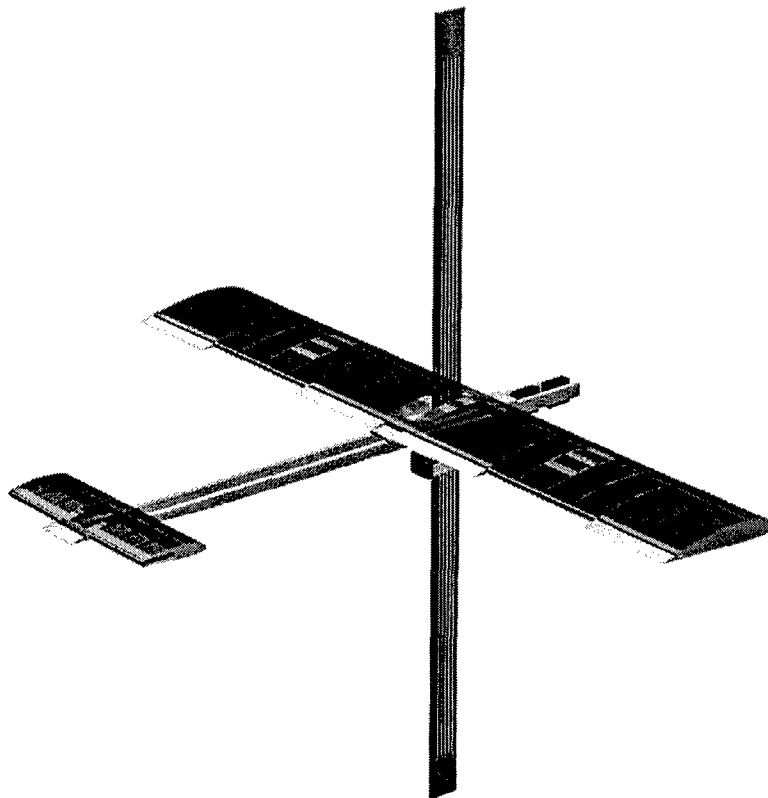


Figure 1 Wind tunnel model with two degrees of freedom (the wing and tail skin is translucent)

The vertical guide rail (for plunging motion) and the hinge (for pitch) are shown in Figure 2. The rail will extend through the height of the test section and its cross section will measure 4 x 0.5 cm. Aerodynamic interference of the carriage will be minimized using a low-weight airfoil-shaped cowling. The pitch mechanism is mounted on the carriage and a slot in the wing allows for smooth change angle of attack. This view also shows the servo-motors that are housed in the nose section. The carriage itself rides on low-friction guides and the vertical rail allows for transfer of low-power electrical signals to the model via an array of copper traces and sliding

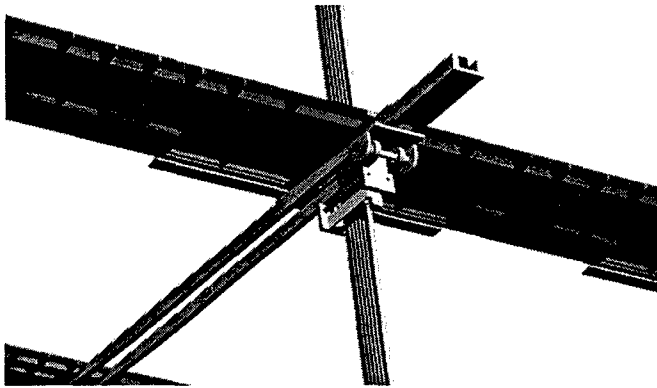


Figure 2 Bottom view of the plunge and pitch mechanisms

contacts. During the fabrication phase the rail will be the subject of early shakedown. Some details of the carriage are shown in Figure 3 (bottom view). The carriage will use light weight ball bearing support and a low-friction axle support through the carriage will allow the pitch motion of the model. The rail bearing system is designed to prevent yaw and roll. A small passive vertical stabilizer can be added to the tail to minimize rail binding and friction.

Details of conventional servo-actuated trailing edge control surface of the wing are shown in Figure 4 (along the segments that are effected by synthetic jet actuators). The movable control surfaces will be hinged using flexible plate inserts for weight saving and simplicity and will be actuated using conventional push rods that will be connected through the fuselage to the servo motors at the nose. As shown in Figure 4, power, control signals for the flow control actuators and the servo control are routed to the model by way of an exposed bus of gold plated PCB traces inlayed into the side of the model support rail. Phosphor-bronze brushes mounted on the model carriage slide along the traces communicate these signals to the model. As noted above, these control surfaces will be used to trim the model so that it floats under its own aerodynamic lift in the wind tunnel's test section before the jet flap flow control actuators are deployed. It is anticipated that the position of the model in the tunnel will be monitored by two or more optical position sensors mounted in the tunnel test section with measurement locations on the fore and aft sections of the fuselage. These time-resolved, high-resolution measurements will yield the instantaneous position of the measurement points and thereby the linear velocity and acceleration. The simultaneous single-point measurements at low angles of attack will provide the time rate of change of the pitch (or angular velocity about the horizontal carriage hinge).

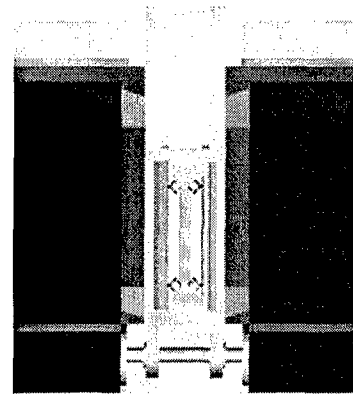


Figure 3 Details of the carriage

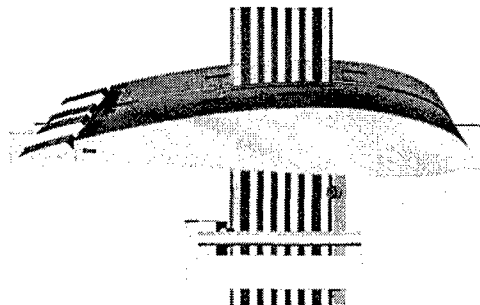


Figure 4 Cross sectional view of the wing and the actuated control surface

2.3 Flow Control Approach

The proposed demonstration vehicle is designed to fly at relatively low speeds for loitering missions where mission duration can be significantly extended by reducing some of the required payload such as batteries and servo hardware. Flow control will be accomplished by using novel, low-power synthetic jet based actuation at the trailing edge of the wing and the tail that will emulate the action of conventional flaps and thereby allow for maneuver without the activation of conventional, servo-powered control surfaces. The aerodynamic forces are derived from interaction between the cross flow and a pairs of adjacent rectangular synthetic jet actuators that are mounted at the trailing edge of the aerodynamic surfaces. As discussed below, the adjacent jets can be continuously vectored in the downstream direction (i.e., into the wake) to emulate the effect a jet-flap without moving control surfaces. The jets are driven by piezoelectric actuators that are selected because of their exceedingly low power consumption, simplicity, and agility. These attributes also enable substantial redundancy and therefore overall improved reliability.

The formation and evolution of two-dimensional synthetic jets was investigated in detail by Smith and Glezer (1997, 1998). A rectangular jet was formed at a high aspect ratio orifice bounding a sealed cavity by the motion of a piezoelectrically-driven membrane mounted on the cavity wall. The authors showed that the flow field of the jet is comprised of two distinct stream wise domains. In the near field immediately downstream of the orifice ($x/L_0 < 0.2$, where L_0 is the characteristic length of the ejected fluid volume), the flow is dominated by the time-periodic alternate formation of counter rotating vortex pairs that are advected away from the orifice and by suction of the makeup fluid into the cavity. In contrast to conventional jets, the vortices that form the synthetic jet do not coalesce but become unstable and break down to form second flow regime of a turbulent jet which in the far field exhibits many of the characteristics of conventional plane jets. As noted by Smith and Glezer (1997), the instantaneous pressure field in the vicinity of the exit plane of a synthetic is substantially modified by the alternate, time periodic, entrainment and vortex formation. The unsteady evolution of the jet flow was exploited by Smith and Glezer for inducing controlled interactions between two adjacent jets. The authors showed that when two high aspect ratio jets are placed side by side, parallel along the lengths of their orifices and spaced about one jet-width apart, the resultant jet can be dynamically manipulated by varying the amplitudes or the relative phase of the driving waveforms. The modification of the evolution of the vortex pairs that form each of the adjacent jets can lead to vectoring of the combined jet as demonstrated in the schlieren images of Figures 5a and b. In these images, the driving signals have the same frequency and amplitude. When the two jets are driven in phase (Figure 5a, $\Delta\phi = 0$), the inner vortices of each vortex pair cancel each other resulting in a single, wider synthetic jet. However, when of the driving signal of the jet on the right is leading in phase (by 60° , Figure 5b), the pressure gradients induced by the blowing and suction strokes of the adjacent actuators and the interactions between the vortex pairs that form each jet lead to vectoring of the combined jet. In Figure 5b, the vortex pair of the jet on the right is formed first while the neighboring actuator is still going through its suction stroke. The interaction between the adjacent vortex pairs (which are no

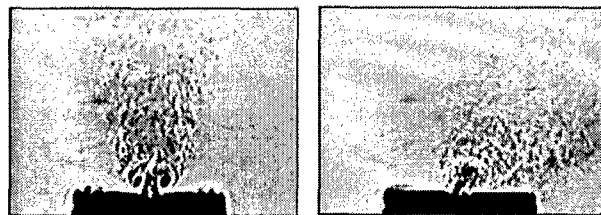


Figure 5 Adjacent synthetic jet $\Delta\phi = 0$ (a) and $\pi/3$ (b)

longer aligned horizontally) and the flow that is induced by the jet actuators alters the vortex pair trajectories and, as a result, the merged jet is vectored towards the actuator that is leading in phase.

The interaction of a synthetic jet (or jet arrays) with an external cross flow over the surface in which they are mounted can displace the local streamlines and induce an apparent or virtual change in the shape of the surface and is therefore of considerable interest for flow control applications. In an investigation of the evolution of synthetic jets on the surface of a 2-D cylinder Honohan et al. (2000) and Glezer et al. (2003, 2005) demonstrated that when the jets are operated on a time scale that is well below the characteristic time scale of the base flow, the formation of a quasi-steady interaction domain near the surface is accompanied by a more favorable pressure gradient. As a result, the surface boundary layer downstream of this domain becomes thinner allowing the flow to overcome stronger adverse pressure gradients and therefore delaying (or altogether suppressing) flow separation.

Of particular interest for the proposed flow control approach is the work of Honohan et al (2003, see also PhD thesis by Honohan, 2004) on the modification of the flow about a circular cylinder by synthetic jet actuation which was demonstrated in a series of low-speed, flow visualization experiments. An image of the baseline flow at $Re_D \approx 7,000$ is shown in Figure 6a. At this Reynolds number, the top and bottom wall boundary layers are laminar and separation occurs at $\theta \approx 85^\circ$. When the jets are placed at the rear stagnation point of the cylinder ($\gamma = 180^\circ$) and the momentum coefficient and jet formation frequencies are relatively high [$C_\mu = O(1)$, $St_D = O(100)$], the effects on the inherently separated base flow is remarkable. When the jets are operated in phase (Figure 6b) the wake is effectively closed, ostensibly due to the transport of fluid from both sides of the cylinder as a result of low pressure induced by the jet. When the adjacent actuators are operated at a phase difference, the resultant jet is vectored (Smith and Glezer, 1998) and the wake is deflected in a manner that is similar to the effect of a jet flap. The resultant flow field over the cylinder (Figure 6c) is reminiscent of potential flow with circulation indicating the presence of lift on the cylinder. This type of control can be applied in a proportional manner by adjusting the magnitude of the phase difference up to approximately $\pm 120^\circ$. Since the actuation frequency is high (three orders of magnitude larger than the Karman vortex shedding frequency), the deflection of the wake is essentially time-invariant.

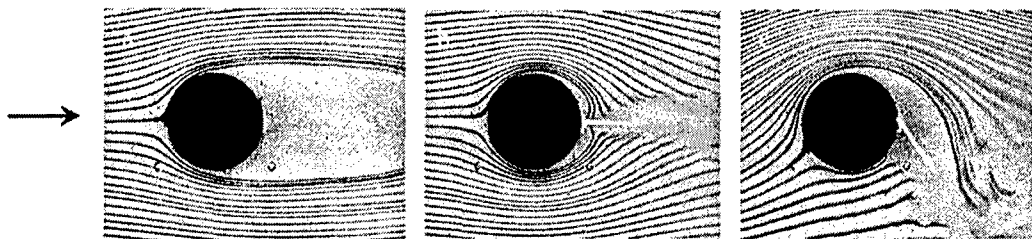


Figure 6 the effect of a pair of synthetic jet actuators on the wake of a cylinder (left to right): a) baseline, b) $\Delta\phi = 0$, and c) $\Delta\phi = \pi/2$. The arrows denote the nominal direction of the combined jet.

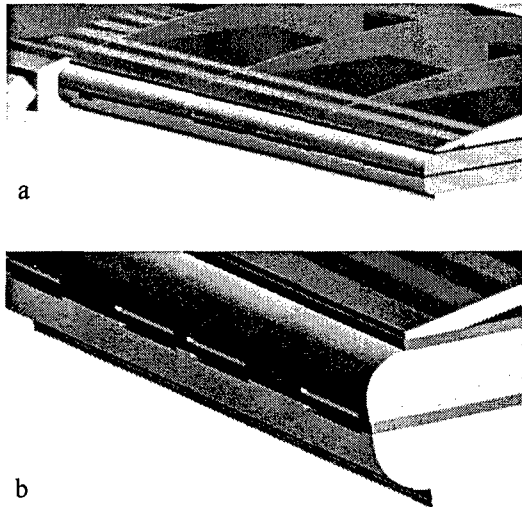


Figure 7 The jet actuator assembly for the proposed UAV configuration: a) mounted at the trailing edge of the wing or tail, and b) a magnified view showing the Coanda surfaces.

This actuation approach will be used to deflect the flow in the near wake of the proposed UAV flight platform. It is anticipated that because the proposed UAV is designed for loitering at inherently low speeds, this approach will be particularly attractive for aerodynamic flow control without moving control surfaces. The Georgia Tech researchers who participated in the STTR program have already demonstrated actuator assemblies of adjacent synthetic jets that are capable of producing momentum coefficient (C_{μ}) on the order of 1-10 at the desired scaling and operating speed for the proposed UAV platform. The proposed design for the present platform is shown in Figure 7. The actuator shell will be structurally integrated with the wing or tail and will utilize new design of piezoceramic drivers that are capable of significant displacement off resonance. An important detail of the design is

the implementation of coanda surfaces near the jet orifices (Figure 7b) to increase the efficiency of the actuator performance at reduced actuation power.

In the proposed Phase II STTR, the dynamics of the interaction between the integrated synthetic jet and the flow over the lifting surfaces (tail and wing) will be characterized in detail using particle image velocimetry (PIV) and the integrated pressure sensors. In particular, the effects of the aerodynamic flow control actuation on the motion of the model (in 2DOF, namely plunge and pitch) will be characterized and optimized and integrated with the adaptive controller that will be developed concurrently and interactively with the wind tunnel investigations.

3. Modeling, Simulation and Control of Test Article

3.1 Abstract

The wind tunnel model (See Section 2.0) proposed for demonstration of flight control using active flow control actuators consists of a main wing and tail. The model will be supported by a traverse mechanism in which motion of the model is constrained to two degrees of freedom. The traverse consists of a vertical beam that passes through middle of the model. The model slides along the beam and has freedom to both pitch and plunge. A conventional elevator is used to trim the model and change its dynamic characteristics. Once the model is trimmed, the position feedback loop is opened, and the elevator controller acts like an inner loop control that alters only the dynamic characteristics, and to introduce disturbances. Once flow control is engaged, position control of the model is achieved by an adaptive outer loop controller that drives the flow actuators. The actuators may be located on the wing and/or on the tail surfaces. If mounted on both surfaces then independent control of pitch and plunge can be explored. For Phase I we model flow control actuation only on the tail surface. Preliminary results are shown that illustrate what can be achieved with the envisioned traverse under both inner and outer loop control.

3.2 Nomenclature

ρ = Air density	$C_{D,t\alpha}$ = Slope of the $C_{D,t}$ versus α curve at $\alpha = 0$
α = Angle of attack	$C_{D,t\delta_e}$ = Slope of the $C_{D,t}$ versus δ_e curve
ϵ = Downwash angle at the tail	$C_{D,t\delta_f}$ = Slope of the $C_{D,t}$ versus δ_f curve
γ = Flight path angle	$C_{D,t0}$ = Zero angle of attack tail drag coefficient
θ = Pitch angle	C_{L0} = Zero angle of attack wing lift coefficient
$\epsilon_0 = \alpha = 0$	C_L = Wing lift coefficient
δ_e = Elevator deflection	$C_{L\alpha}$ = Slope of the C_L versus α curve at $\alpha = 0$
δ_{e0} = Trim elevator deflection	$C_{L,t}$ = Tail lift coefficient
δ_i = Inner loop control elevator deflection	$C_{L,t\alpha}$ = Slope of the $C_{L,t}$ versus α curve at $\alpha = 0$
$\eta_s = S_i/S$ = Ratio of tail area to wing area	$C_{L,t\dot{\alpha}}$ = Slope of the $C_{L,t}$ versus normalized $\dot{\alpha}$ curve
δ_f = Active flow control signal	
$\eta_t = (V'/V)^2$ = Tail efficiency factor	
\bar{c} = Wing chord length	
C_D = Wing drag coefficient	
$C_{D\alpha}$ = Slope of the C_D versus α curve at $\alpha = 0$	
$C_{D,t}$ = Tail drag coefficient	

$C_{L,t\delta_e}$	Elevator effectiveness (slope of the $C_{L,t}$ versus δ_e curve)	L_w	Aerodynamic lift force acting on the wing
$C_{L,t\delta_f}$	Active flow control actuator effectiveness (slope of the $C_{L,t}$ versus δ_f curve)	m	Mass of the model
$C_{L,t0}$	Zero angle of attack tail lift coefficient	P	Point where the model is attached to the support mechanism (assumed to be coincident with the wing aerodynamic center)
$C_{L,tq}$	Slope of the $C_{L,t}$ versus normalized q curve at	$q = \frac{1}{2}\rho V_0^2$	Dynamic pressure
C_{L0}	Zero angle of attack wing lift coefficient	S	Wing surface area
I	Moment of inertia of the model around P	S_t	Tail surface area
l	Distance from the tail aerodynamic center to P	V	Air speed experienced by the model
l_g	Distance from the model center of gravity to P	$= \sqrt{V_0^2 + \dot{z}^2}$	
L_t	Aerodynamic lift force acting on the tail	V'	Effective air speed at tail
		V_0	Speed of the wind tunnel
		z	Vertical position of the model

3.3 Introduction

A primary objective of this project was to demonstrate closed loop adaptive flow control under a highly dynamic flight condition. The wind tunnel model for this project has been designed based on conventional flight control principles. The actual construction of the model and its suspension mechanism will take place during Phase II. A low-weight model will be manufactured so that aerodynamic forces alone will be sufficient to support the model in the tunnel. To constrain the motion of the model to plunging and pitching, a low friction beam will be installed along the vertical direction through the wing. This beam will prevent the model from rolling and yawing, and will allow it to slide up and down and pitch with nearly zero friction.

3.4 Passive Traverse Design and Equations of Motion

A free body diagram of the model is shown in Figure 8. The model is constrained by the beam at point P , which is assumed to be at the aerodynamic center of the wing. It is further assumed that the beam can only exert horizontal forces to the model, which cancel the horizontal component of the aerodynamic forces. The dynamics and control problem is very similar to that encountered in conventional longitudinal aircraft control. Plunging and pitching dynamics can be written as

$$\begin{aligned} mg - L_w \cos \gamma - L_t \cos(\gamma - \varepsilon) - D_w \sin \gamma - D_t \sin(\gamma - \varepsilon) &= m\ddot{z} \\ (L_w \cos \gamma + D_w \sin \gamma)l_g \cos \theta - [L_t \cos(\gamma - \varepsilon) + D_t \sin(\gamma - \varepsilon)](l - l_g) \cos \theta &= I\ddot{\theta} \end{aligned} \quad (1)$$

where ε is the downwash angle of the flow as seen at the tail surface. The flight path angle is given by

$$\gamma = \tan^{-1} \left(\frac{\dot{z}}{V_0} \right) \quad (2)$$

Aerodynamic Forces

Pitching and plunging motion are controlled by changing the lift on the tail. To this end, we assume that lift on the tail can be varied by using both a moving elevator surface and flow actuators located on the tail surface. We write lift and drag on wing and tail as

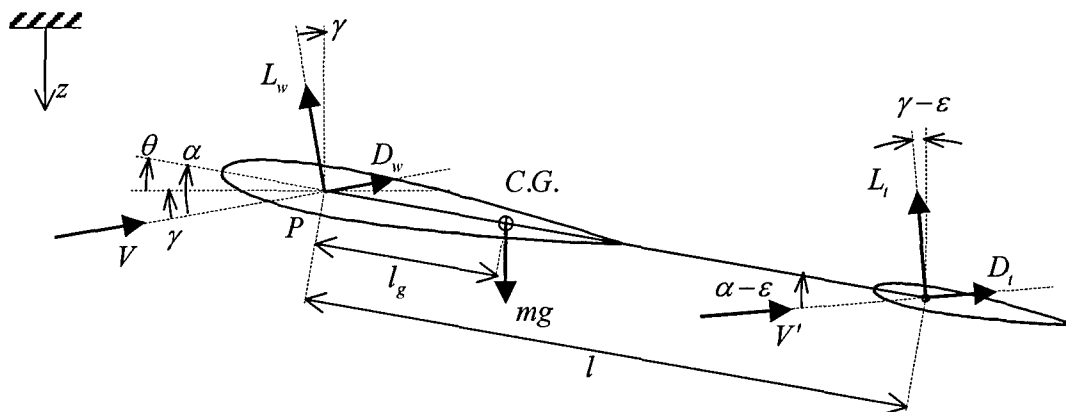


Figure 8. Free-body diagram of the 2-DOF wind tunnel model.

$$\begin{aligned}
L_w &= qS (C_{L_0} + C_{L_\alpha} \alpha) \\
D_w &= qS (C_{D_0} + C_{D_\alpha} \alpha) \\
L_t &= qS \eta_s \eta_t \left(C_{L,t_0} + C_{L,t_\alpha} (\alpha - \varepsilon) + C_{L,t_\alpha} (\dot{\alpha} - \dot{\varepsilon}) \frac{\bar{c}}{2V_0} + C_{L,t_q} q \frac{\bar{c}}{2V_0} + C_{L,t_{\delta_e}} \delta_e + C_{L,t_{\delta_f}} \delta_f \right) \\
D_t &= qS \eta_s \eta_t \left(C_{D,t_0} + C_{D,t_\alpha} (\alpha - \varepsilon) + C_{D,t_{\delta_e}} \delta_e + C_{D,t_{\delta_f}} \delta_f \right)
\end{aligned} \tag{3}$$

where $q = \frac{1}{2} \rho V^2$ is the dynamic pressure and $\eta_s = S_t/S$ and $\eta_t = (V'/V)^2$. The downwash ε can be closely approximated as a linear function of α

$$\varepsilon = \varepsilon_0 + \frac{\partial \varepsilon}{\partial \alpha} \alpha \tag{4}$$

Using (4) in (3), we can express the aerodynamic forces as:

$$\begin{aligned}
L_w &= qS (C_{L_0} + C_{L_\alpha} \alpha) \\
D_w &= qS (C_{D_0} + C_{D_\alpha} \alpha) \\
L_t &= qS \eta_s \eta_t \left(C_{L,t_0} - C_{L,t_\alpha} \varepsilon_0 + C_{L,t_\alpha} \left(1 - \frac{\partial \varepsilon}{\partial \alpha}\right) \alpha + C_{L,t_\alpha} \left(1 - \frac{\partial \varepsilon}{\partial \alpha}\right) \dot{\alpha} \frac{\bar{c}}{2V_0} + C_{L,t_q} q \frac{\bar{c}}{2V_0} + C_{L,t_{\delta_e}} \delta_e + C_{L,t_{\delta_f}} \delta_f \right) \\
D_t &= qS \eta_s \eta_t \left(C_{D,t_0} - C_{D,t_\alpha} \varepsilon_0 + C_{D,t_\alpha} \left(1 - \frac{\partial \varepsilon}{\partial \alpha}\right) \alpha + C_{D,t_{\delta_e}} \delta_e + C_{D,t_{\delta_f}} \delta_f \right)
\end{aligned} \tag{5}$$

Redefining the tail aerodynamic coefficient so that the effect of the downwash angle is included:

$$\begin{aligned}
C_{L,t_0} &= C_{L,t_0} - C_{L,t_\alpha} \varepsilon_0 \\
C_{D,t_0} &= C_{D,t_0} - C_{D,t_\alpha} \varepsilon_0 \\
C_{L,t_\alpha} &= C_{L,t_\alpha} \left(1 - \frac{\partial \varepsilon}{\partial \alpha}\right) \\
C_{L,t_\alpha} &= C_{L,t_\alpha} \left(1 - \frac{\partial \varepsilon}{\partial \alpha}\right) \\
C_{D,t_\alpha} &= C_{D,t_\alpha} \left(1 - \frac{\partial \varepsilon}{\partial \alpha}\right)
\end{aligned} \tag{6}$$

then the expressions in (5) can be simplified to read

$$\begin{aligned}
L_w &= qS(C_{L_0} + C_{L_\alpha}\alpha) \\
D_w &= qS(C_{D_0} + C_{D_\alpha}\alpha) \\
L_t &= qS\eta_s\eta_t \left(C_{L,t_0} + C_{L,t_\alpha}\alpha + C_{L,t_{\dot{\alpha}}}\dot{\alpha}\frac{\bar{c}}{2V_0} + C_{L,t_q}q\frac{\bar{c}}{2V_0} + C_{L,t_{\delta_e}}\delta_e + C_{L,t_{\delta_f}}\delta_f \right) \\
D_t &= qS\eta_s\eta_t \left(C_{D,t_0} + C_{D,t_\alpha}\alpha + C_{D,t_{\delta_e}}\delta_e + C_{D,t_{\delta_f}}\delta_f \right)
\end{aligned} \tag{7}$$

Linearization

The equations of motion derived in the previous section are linearized for the inner loop control design using small-disturbance theory. We assume a trim condition with $z = z_0$, $\dot{z} = 0$, $\theta = \theta_0$, $\dot{\theta} = 0$ and consider the motion as small deviations from this reference steady condition. Since trim conditions for \dot{z} , and $\dot{\theta}$ are zero, and the dynamics are independent of z_0 , these variables are redefined as representing small perturbations from equilibrium. For pitch angle we will use $\theta = \theta_0 + \Delta\theta$ where θ_0 is the equilibrium value and $\Delta\theta$ is a small perturbation. Similarly for vertical position and elevator deflection we will use $z = z_0 + \Delta z$ and $\delta_e = \delta_{e_0} + \Delta\delta_e$. The following approximations will be used for the nonlinear terms:

$$\begin{aligned}
\alpha &\cong \theta_0 + \theta + \frac{\dot{z}}{V_0} & \dot{\alpha} &\cong \dot{\theta} + \frac{\ddot{z}}{V_0} \\
\cos\theta &\cong \cos\theta_0 - \theta\sin\theta_0 & \sin\theta &\cong \theta\cos\theta_0 + \sin\theta_0 \\
q &\cong \frac{1}{2}\rho(V_0 + \dot{z})^2 = \frac{1}{2}\rho V_0^2 & \sin\gamma &\cong \frac{\dot{z}}{V_0} & \cos\gamma &\cong 1
\end{aligned} \tag{8}$$

For simplicity we further assume $C_{L,t_{\dot{\alpha}}} = 0$ for the linear model. These approximations and the assumption that products of small perturbations are zero lead to the following linearization of (1)

$$\begin{aligned}
m\ddot{z} &= mg - (L_w + L_t) - (D_w + D_t)\frac{\dot{z}}{V_0} \\
I\ddot{\theta} &= L_w l_g \cos\theta_0 - L_w l_g \sin\theta_0 \Delta\theta + \frac{D_w}{V_0} \cos\theta_0 l_g \dot{z} - L_t (l - l_g) \cos\theta_0 + \\
&L_t (l - l_g) \sin\theta_0 \Delta\theta - \frac{D_t}{V_0} (l - l_g) \cos\theta_0 \dot{z}
\end{aligned} \tag{9}$$

Trimming

We assume that elevator command contains a bias term to trim the model at the equilibrium point with all the perturbations at zero. The equilibrium pitch angle θ_0 needed to balance the model for a given mass and tunnel speed, and the elevator command δ_{e_0} to hold the pitch attitude

at that level can be found from the simultaneous solution of equations (9) after equating all the perturbations to zero:

$$\begin{aligned} \frac{mg}{qS} - (C_{L_0} + \eta_s \eta_l C_{L,l_0}) &= (C_{L_\alpha} + \eta_s \eta_l C_{L,l_\alpha}) \theta_0 + \eta_s \eta_l C_{L,l_{\delta_e}} \delta_{e0} \\ -C_{L_0} l_g + \eta_s \eta_l C_{L,l_0} (l-l_g) &= [C_{L_\alpha} l_g - \eta_s \eta_l C_{L,l_\alpha} (l-l_g)] \theta_0 - \eta_s \eta_l C_{L,l_{\delta_e}} (l-l_g) \delta_{e0} \end{aligned} \quad (10)$$

Since these equations and the values of the parameters are approximate, trim values for the actual experiment setup will need to be obtained by a closed loop controller during the experiment.

Finally, defining the states as $x_1 = \Delta z$, $x_2 = \dot{z}$, $x_3 = \Delta \theta$, and $x_4 = \dot{\theta}$, and inserting the aerodynamic forces from (7) and ignoring the products of perturbations we obtain the linear system model as

$$\begin{bmatrix} \dot{x}_1 \\ \dot{x}_2 \\ \dot{x}_3 \\ \dot{x}_4 \end{bmatrix} = \begin{bmatrix} 0 & 1 & 0 & 0 \\ 0 & a_{2,2} & a_{2,3} & a_{2,4} \\ 0 & 0 & 0 & 1 \\ 0 & a_{4,2} & a_{4,3} & a_{4,4} \end{bmatrix} \begin{bmatrix} x_1 \\ x_2 \\ x_3 \\ x_4 \end{bmatrix} + \begin{bmatrix} 0 \\ b_{e,2} \\ 0 \\ b_{e,4} \end{bmatrix} \delta_e + \begin{bmatrix} 0 \\ b_{f,2} \\ 0 \\ b_{f,4} \end{bmatrix} \delta_f \quad (11)$$

with

$$\begin{aligned} a_{2,2} &= -\frac{qS}{V_0 m} (C_{L_\alpha} + C_{D_0} + C_{D_\alpha} \theta_0 + \eta (C_{L,l_\alpha} + C_{D,l_0} + C_{D,l_\alpha} \theta_0 + C_{D,l_{\delta_e}} \delta_{e0})) \\ a_{2,3} &= -\frac{qS}{m} (C_{L_\alpha} + \eta C_{L,l_\alpha}) \\ a_{2,4} &= -\frac{qS}{2V_0 m} \eta \bar{c} (C_{L,l_\alpha} + C_{L,l_q}) \\ a_{4,2} &= \frac{qS}{V_0 I} \left[\begin{aligned} &(C_{L_\alpha} + C_{D_0} + C_{D_\alpha} \theta_0) l_g \\ &- \eta (C_{L,l_\alpha} + C_{D,l_0} + C_{D,l_\alpha} \theta_0 + C_{D,l_{\delta_e}} \delta_{e0}) (l-l_g) \end{aligned} \right] \cos \theta_0 \\ a_{4,3} &= \frac{qS}{I} \left[\begin{aligned} &\eta (C_{L,l_0} + C_{L,l_\alpha} \theta_0 + C_{L,l_{\delta_e}} \delta_{e0}) (l-l_g) - l_g (C_{L_0} + C_{L_\alpha} \theta_0) \\ &+ [C_{L_\alpha} l_g - \eta C_{L,l_\alpha} (l-l_g)] \cos \theta_0 \end{aligned} \right] \sin \theta_0 \\ a_{4,4} &= -\frac{qS}{2V_0 I} \eta \bar{c} (C_{L,l_\alpha} + C_{L,l_q}) (l-l_g) \cos \theta_0 \end{aligned}$$

$$\begin{aligned}
b_{e,2} &= -\frac{qS}{m} \eta C_{L,i,\delta_e} \\
b_{e,4} &= -\frac{qS}{I} \eta C_{L,i,\delta_e} (l-l_g) \cos \theta_0 \\
b_{f,2} &= -\frac{qS}{m} \eta C_{L,i,\delta_i} \\
b_{f,4} &= -\frac{qS}{I} \eta C_{L,i,\delta_e} (l-l_g) \cos \theta_0
\end{aligned}$$

We will write the linear system model in the following compact form for controller design:

$$\dot{x} = Ax + b_e \delta_e + b_f \delta_f \quad (12)$$

3.5 Controller Design

The controller output has two components, one for regulating the elevator and one for regulating the flow control devices. The elevator portion command includes two components:

$$\delta_e = \delta_{e0} + \delta_i \quad (13)$$

where δ_{e0} is the trim command. We refer to this as the inner loop component because in normal operation (when the flow control devices are activated) the elevator control has its position feedback loop open. The flow controller forms the outer loop portion of the controller, which we denote as δ_f . At the start of the experiment, only the trim controller will be active, which is basically an LQR controller augmented by an integrator. When the model reaches the trim condition, the integrator state of this controller will be frozen and forms the δ_{e0} term in (13). At the same time the position feedback loops are opened, and the LQR controller that remains is the δ_i term in (13). Shortly afterwards the outer loop controller will be engaged, which will be designed as a linear compensator augmented with an integrator and an adaptive element. Opening the position feedbacks of the inner loop controller will ensure that the model position will be completely regulated by the adaptive outer loop controller using the active flow actuators. If in addition we install flow control devices on the wing, then we should be able to independent regulate position and attitude. For controller design we assume full state feedback information is available, consisting of vertical position, pitch attitude, and their derivatives.

Trim controller design

Finding the trim condition and the required elevator trim deflection requires integral action on the vertical position. To incorporate integrator design into the LQR design, we augment the linear model (12) with an auxiliary state x_i as the integral of x_1 as

$$\dot{\tilde{x}} = \begin{bmatrix} \dot{x} \\ \dot{x}_i \end{bmatrix} = \begin{bmatrix} A & 0 \\ c_1 & 0 \end{bmatrix} \tilde{x} + \begin{bmatrix} b_e \\ 0 \end{bmatrix} \delta_e + \begin{bmatrix} b_f \\ 0 \end{bmatrix} \delta_f \quad (14)$$

where $c_1 = [1 \ 0 \ 0 \ 0]$. LQR controller design based on the above augmented model returns the gain matrix $K_i = [k_{i,1} \ k_{i,2} \ k_{i,3} \ k_{i,4} \ k_{i,5}]$ where $k_{i,1}$ through $k_{i,4}$ are gains on states x_1 through x_4 respectively, and $k_{i,5}$ is the gain for the integral of vertical position. Trim controller in transient is $\delta_{e0} = -K_i \bar{x}$. When steady state is reached, δ_{e0} will be frozen and remain constant throughout the experiment.

Inner loop controller design

The inner loop controller is simply the LQR controller designed for trim with integrator and position feedbacks removed:

$$\delta_i = -K_i x \quad (15)$$

where $K_i = [0 \ k_{i,2} \ 0 \ k_{i,4}]$. Closing the inner loop leads to the linear system

$$\dot{x}_m = A_m x_m + b_f \delta_f \quad (16)$$

with $A_m = A - B_e K_i$ and x_m indicating the state vector of the linear model with inner loop closed, which will be used as the plant model for the outer loop controller design.

Outer loop controller design

The outer loop controller will be composed of a linear controller augmented with an adaptive neural network (NN). The linear part will be an LQR controller augmented by an integrator, similar to the trim controller in transient. To compensate for the modelling errors, unmodeled dynamics, and nonlinearities of the flow actuators, an adaptive NN will be introduced following the method of [5] as

$$\delta_f = \delta_{ec} - \delta_{NN} \quad (17)$$

To this end, we introduce a state transformation $\xi_m = T x_m$ to transform the plant model into normal form as

$$\begin{aligned} \dot{\xi}_m &= A_n \xi_m + b_n \delta_f \\ \xi_m &= T x_m \end{aligned} \quad (18)$$

where $A_n = T A_m T^{-1}$ and $b_n = T b_f$. Note that the above model in normal form can also be written in the same form as the plant model in [5] as

$$\begin{aligned}
\dot{z}_l &= F_0 z_l + g_0 x_l \\
\dot{x}_1 &= x_2 \\
&\vdots \\
\dot{x}_r &= h_0^T z_l + a_1 x_1 + \dots + a_r x_r + b \delta_f \\
y_l &= x_1
\end{aligned} \tag{19}$$

with $\xi_m = [z_l \ x_l]^T = [z_l \ [x_1 \ \dots \ x_r]]^T$, where z_l represents the states of the internal dynamics and x_l represents the feedback linearized states. Note that the conventional longitudinal control of an airplane from tail is inherently a non-minimum phase system, which means that the matrix F_0 in (19) is not Hurwitz.

Linear compensator design for the outer loop

Linear compensator for the outer loop is designed in the same way as the trim controller discussed previously. We first augment the model in (18) with an auxiliary state for the integral of the vertical position as

$$\dot{\bar{\xi}}_m = \begin{bmatrix} A_n & 0 \\ c_1 & 0 \end{bmatrix} \bar{\xi}_m + \begin{bmatrix} b_n \\ 0 \end{bmatrix} \delta_f \tag{20}$$

We obtain the full state feedback gain $K_o = [k_{o,1} \ k_{o,2} \ k_{o,3} \ k_{o,4} \ k_{o,5}]$ from the LQR design. This time we leave all the feedbacks closed, including the integral term:

$$\delta_{ec} = -K_o \bar{\xi}_m \tag{21}$$

Error dynamics

Based on the linear plant model (19), we write the true system dynamics as

$$\begin{aligned}
\dot{z} &= F_0 z + g_0 x_1 + \Delta_2 \\
\dot{x}_1 &= x_2 \\
&\vdots \\
\dot{x}_r &= h_0^T z + a_1 x_1 + \dots + a_r x_r + b(\delta_f + \Delta_1) \\
y &= x_1
\end{aligned} \tag{22}$$

where Δ_1 is the portion of the modelling error that lies in the range space of the control and Δ_2 is the modelling error in internal dynamics that satisfies a linear growth condition as detailed in (1). The plant in (22) under the regulation of (17) along with (21) can be written as

$$\dot{\bar{\xi}} = \underbrace{\left(\begin{bmatrix} A_n & 0 \\ c_1 & 0 \end{bmatrix} - \begin{bmatrix} b_n \\ 0 \end{bmatrix} K_o \right)}_{\bar{a}} \bar{\xi} + \underbrace{\begin{bmatrix} b_n \\ 0 \end{bmatrix}}_{\bar{b}} (-\delta_{NN} + \Delta_1) + \begin{bmatrix} \Delta_2 \\ 0 \end{bmatrix} \tag{23}$$

Defining the error vector as $E = \bar{\xi}_m - \bar{\xi}$, we can write the error dynamics as

$$\dot{E} = \bar{A}E + \bar{b}(\delta_{NN} - \Delta_1) - \bar{\Delta}_2 \quad (24)$$

Adaptive NN design for the outer loop

Following [5], a single hidden layer neural network (SHLNN) is introduced as

$$\delta_{NN} = \hat{M}^T \sigma(\hat{N}^T \eta) \quad (25)$$

where the adaptive gain matrices \hat{M} and \hat{N} are updated according to the following laws:

$$\begin{aligned} \dot{\hat{M}} &= -F \left[(\hat{\sigma} - \hat{\sigma}' \hat{N}^T \eta) E^T P \bar{b} + k \hat{M} \right] \\ \dot{\hat{N}} &= -G \left[\eta E^T P \bar{b} \hat{M}^T \hat{\sigma}' + k \hat{N} \right] \end{aligned} \quad (26)$$

where $\eta = [\delta, \bar{\xi}^T]^T$ is the input vector to the NN, $\hat{\sigma} = \sigma(\hat{N}^T \eta)$, $\hat{\sigma}'$ is the Jacobian computed at the estimates, and P is the solution to the Lyapunov equation

$$\bar{A}^T P + P \bar{A} = -Q$$

with some $Q \succ 2I$. As proven in [5], the controller (17) and (25) along with (26) guarantees that the error states E remain bounded as long as the system initially starts from within a compact set defined in [5].

Control Hedging

A novel method known as control hedging (CH) for protecting the adaptive controller from known actuator characteristics has been demonstrated in [6] in the setting of augmenting a linear controller. CH prevents an adaptive element from attempting to adapt to input nonlinearities by incorporating an actuator model to remove these nonlinearities in the error dynamics. Hedging has successfully been implemented in various numerical and experimental works. In particular, it has been shown to help adaptation to continue correctly in cases of actuators with hysteresis type of nonlinearity [7] and discrete actuation with exponential rise and decay profiles [8]. Both of these types of nonlinearities are likely to be encountered in active flow actuators. Therefore, CH is a crucial component of the adaptive controller in this effort. An approximate model of the flow control actuators that include the key physical characteristics will be derived and used in the CH loop to protect adaptation from their effects.

3.6 Actuator Modeling

Realistic models for both the elevator and active flow control actuator are required to evaluate the adaptive controllers in simulation.

Elevator model

Based on off-the-shelf servo specifications, elevator is modelled as a first order system with

$$G_e(s) = \frac{\delta_e(s)}{\delta_{e,com.}(s)} = \frac{15}{s+15}$$

where $\delta_{e,com.}(s)$ is the commanded deflection. Also magnitude of the elevator deflection is limited to be less than 45 deg.

Active Flow Actuator Model

Active flow control actuators tested in a wind tunnel in a static flight condition exhibit a dynamic response as shown in Figure 9. The incremental change in circulation (with respect to the baseline flow) about a stalled 2-D airfoil is shown in Figure 9 (a). An adverse change in circulation is observed immediately following the start of the actuation, similar to the response of a non-minimum phase system to a step input. Flow visualization images showing the transient actuation are presented in Figure 9 (b). To model this transient behavior, a non-minimum phase transfer function is introduced

$$G_f(s) = \frac{\delta_f(s)}{\delta_{f,com.}(s)} = \frac{-100(s-100)}{(s+100)^2}$$

where $\delta_{f,com.}(s)$ is the commanded actuation. Response of the above model to a step input is also shown in Figure 9 (c).

The response in Figure 9(a) represent actuation in a stationary flow condition. Behavior of active flow actuators in a dynamic flight condition is yet to be investigated. In an attempt to represent possible coupling effects between actuation, the dynamics of flow field, and the rigid body dynamics of the model we propose the following model for the flow actuator effectiveness coefficient C_{L,s_f} :

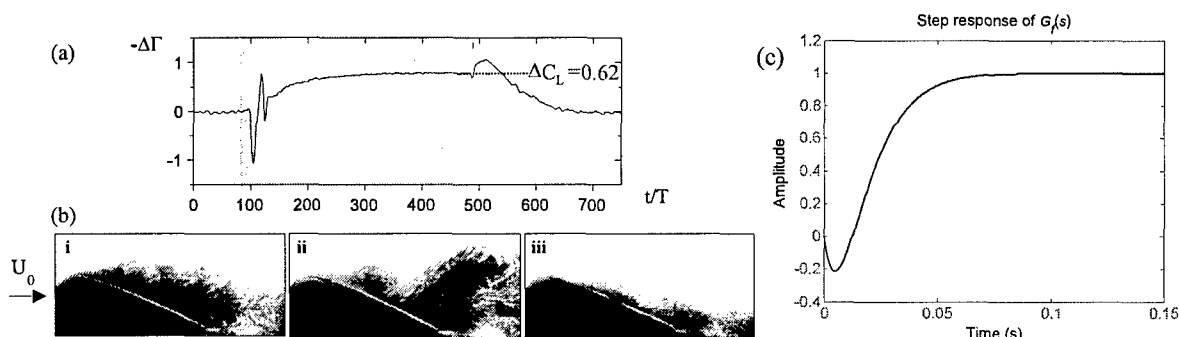


Figure 9. Transient control with an active flow actuator: a) Time history of the circulation when control is activated, b) Flow visualization images during flow reattachment: i. separated flow, ii. collapse of the separation domain, and iii. beginning of full reattachment, and (c) Step response of $G_f(s)$.

$$C_{L,\delta_f} = C_{L,\delta_{f0}} + C_{L,\delta_{f\alpha}} \alpha + C_{L,\delta_{f\alpha^2}} \alpha^2 + C_{L,\delta_{f\dot{\alpha}}} \dot{\alpha} + C_{L,\delta_{f\theta}} \theta + C_{L,\delta_{f\dot{\theta}}} \dot{\theta}$$

The structure and parameters of this model will be adjusted to replicate as close as possible the experimentally obtained open loop frequency response and time response data, once it is available. For the simulation results presented below, each of these parameters has been selected to have an adverse effect on the closed loop response. This selection therefore represents a hypothetical worst case situation.

3.7 Simulation Results

We present simulation results with two different inner loop controller designs, comparing the responses with and without adaptation for each case. Linear controller designs for the inner and outer loops ignore the actuator models. In addition, we introduce uncertainties to aerodynamic parameters as summarized in Table 1. Similar to selection of the flow actuator model parameters, uncertainties in these variables are selected to represent a hypothetical worst case.

Case 1

First the inner loop controller is designed to make the model have satisfactory damping. The intended pole locations and the actual pole locations, which are different due to the uncertainties introduced in Table 1, are given in Table 2. We see that the uncertainties have a significant effect on the closed loop dynamics. Recall that the inner loop controller is used to trim the model, and then its position feedback loop is opened. At this point the outer, flow-control loop is engaged. Simulation results without adaptation in the outer loop are shown in Figure 10. The simulation starts with zero initial conditions. The model is trimmed using the inner loop trim controller in the first ten seconds. At $t = 10$ s, the trim setting is held fixed, and the position feedback loop of the inner loop controller is opened, and the outer loop controller without adaptation is engaged. The flow control actuator causes the highly oscillatory response observed.

Results for this case with adaptation are presented in Figure 11. Adaptation successfully removes the oscillations.

Case 2

Gains on the velocity feedbacks for the inner loop controller are modified manually to lower the damping of the model. Intended and actual pole locations are shown in Table 2. Results without adaptation are in Figure 12. The system quickly goes unstable when the outer loop controller is engaged. With adaptation, system remains stable as seen in Figure 13. The response is very similar to the case with high damping, which shows that adaptation can handle significant changes in system dynamics.

Table 1. Aerodynamic parameters.

Linear Model		True Plant	
ε_0	= 0	ε_0	= -0.05
$\frac{\partial \varepsilon}{\partial \alpha}$	= 0.05 rad ⁻¹	$\frac{\partial \varepsilon}{\partial \alpha}$	= 0.05 rad ⁻¹
η_s	= 0.42	η_s	= 0.42
η_t	= 1	η_t	= 0.75
\bar{c}	= 0.4 m	\bar{c}	= 0.4 m
C_{D_α}	= 4.27 rad ⁻¹	C_{D_α}	= 6.41 rad ⁻¹
$C_{D,\dot{\alpha}}$	= 4.06 rad ⁻¹	$C_{D,\dot{\alpha}}$	= 6.08 rad ⁻¹
$C_{D,\dot{\delta}_e}$	= 0.03 rad ⁻¹	$C_{D,\dot{\delta}_e}$	= 0.05 rad ⁻¹
$C_{D,\dot{\delta}_0}$	= 0.1	$C_{D,\dot{\delta}_0}$	= 0.15
C_{L_0}	= 0	C_{L_0}	= 0
C_{L_α}	= 5.73 rad ⁻¹	C_{L_α}	= 4.30 rad ⁻¹
$C_{L,\dot{\alpha}}$	= 5.44 rad ⁻¹	$C_{L,\dot{\alpha}}$	= 4.08 rad ⁻¹
$C_{L,\dot{\alpha}^2}$	= 0	$C_{L,\dot{\alpha}^2}$	= -5 rad ⁻¹
$C_{L,\dot{\delta}_e}$	= 1 rad ⁻¹	$C_{L,\dot{\delta}_e}$	= 0.75 rad ⁻¹
$C_{L,\dot{\delta}_0}$	= 0	$C_{L,\dot{\delta}_0}$	= 0
$C_{L,\dot{q}}$	= 8.5 rad ⁻¹	$C_{L,\dot{q}}$	= 6.38 rad ⁻¹
I	= 0.1 kg.m ²	I	= 0.15 kg.m ²
l	= 0.75 m	l	= 0.56 m
l_g	= 0.1 m	l_g	= 0.13 m
m	= 1 kg	m	= 0.75 kg
V_0	= 10 m/s	V_0	= 10 m/s

Table 2. Inner loop and outer loop linear controller designs.

	Intended inner loop poles, $\hat{\lambda}(A_m)$	Actual inner loop poles, $\lambda(A_m)$	Intended outer loop poles $\hat{\lambda}(\bar{A})$	Actual outer loop poles $\lambda(\bar{A})$
Case 1: High damping	0 -5.20 -7.41 -58.75	0 -4.04 + 4.55i -4.04 - 4.55i -13.89	-1.07 -1.85 -7.41 + 3.01i -7.41 - 3.01i -65.01	-1.12 -1.50 -4.29 + 9.89i -4.29 - 9.89i -13.03
Case 2: Low damping	0 -6.29 + 10.02i -6.29 - 10.02i -52.81	0 -1.31 + 10.78i -1.31 - 10.78i -14.26	-0.89 + 0.45i -0.89 - 0.45i -7.39 + 9.24i -7.39 - 9.24i -59.30	-1.07 + 0.19i -1.07 - 0.19i -1.98 + 12.22i -1.98 - 12.22i -13.86

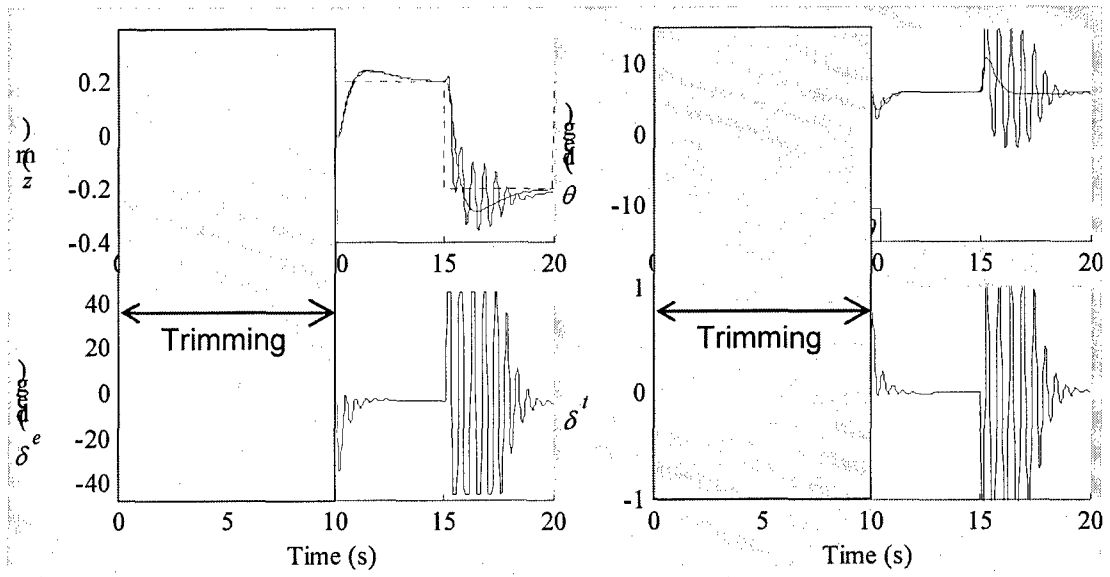


Figure 10. Simulation results, Case 1, without adaptation.

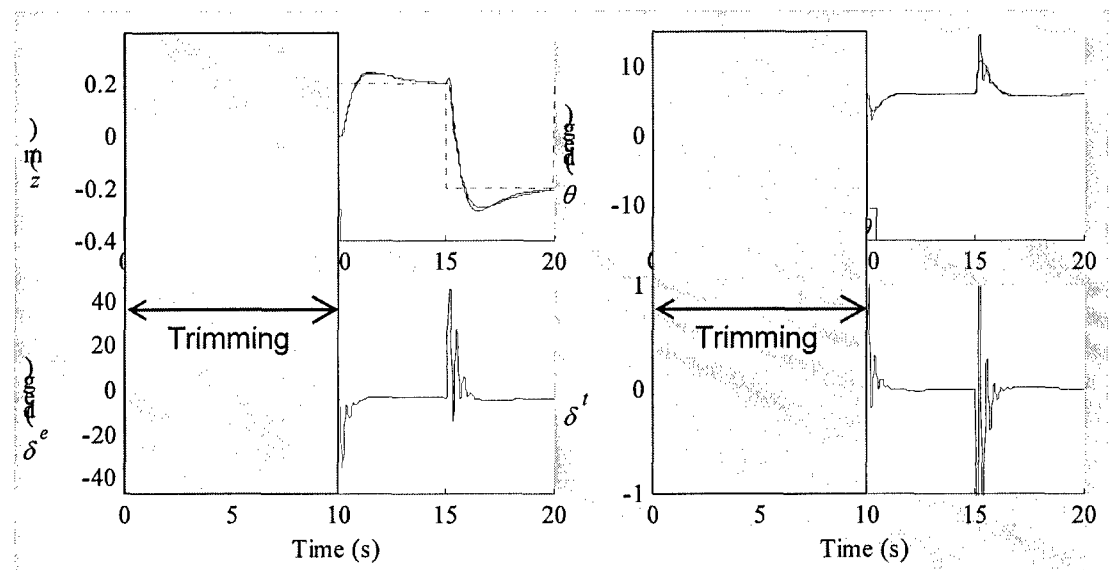


Figure 11. Simulation results, Case 1, with adaptation.

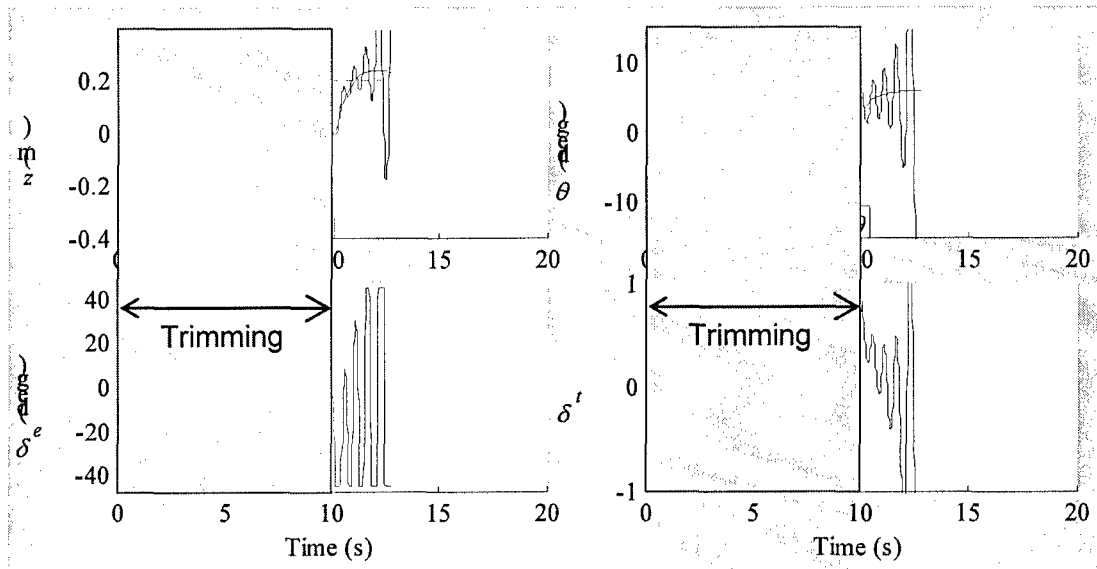


Figure 12. Simulation results, Case 2, without adaptation.

4.

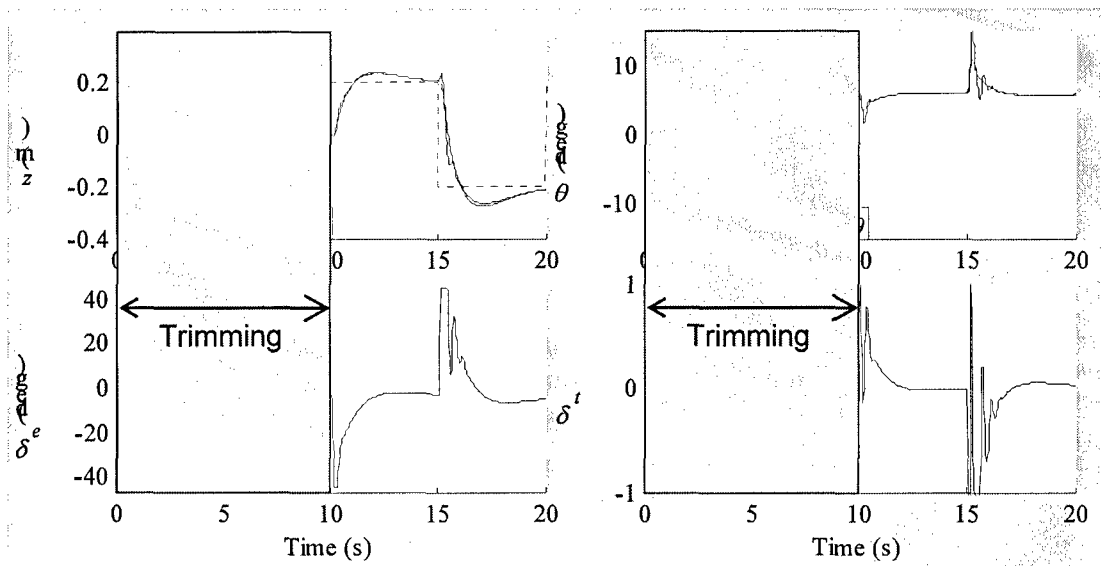


Figure 13. Simulation results, Case 2, with adaptation.

4. Summary, Conclusions and Recommendations

The objective of this research program is to develop and demonstrate effective nonlinear adaptive control of the aerodynamic flow about a dynamic body using a distributed array of synthetic jets for actuation. The phase I STTR program reported herein conceived of and completed preliminary design of a wind-tunnel test apparatus for demonstration of adaptive flow control under dynamic flight conditions in both the wind tunnel and flight. In the wind tunnel, the model will be supported by a traverse mechanism in which motion of the model is constrained to two degrees of freedom. The traverse consists of a vertical beam that passes through middle of the model. The model slides along the beam and has freedom to both pitch and plunge. A conventional elevator is used to trim the model and change its dynamic characteristics. Once the model is trimmed, the position feedback loop is opened, and the elevator controller acts like an inner loop control that alters only the dynamic characteristics, and to introduce disturbances. Once flow control is engaged, position control of the model is achieved by an adaptive outer loop controller that drives the flow actuators. The actuators may be located on the wing and/or on the tail surfaces. If mounted on both surfaces then independent control of pitch and plunge can be explored. For Phase I we modeled flow control actuation only on the tail surface. Preliminary results are shown that illustrate what can be achieved with the envisioned traverse under both inner and outer loop control.

A dynamic simulation model of the wind tunnel apparatus was developed and coded. Inner and outer loop controllers were designed for this system, the outer loop being adaptive. A non-minimum phase transfer function was introduced to model the active flow control actuators based on wind tunnel experience in stationary flow conditions. Behavior of active flow actuators in a dynamic flight condition has yet to be investigated. The model employed for the flow actuator effectiveness coefficient included possible coupling effects between actuation, the dynamics of flow field, and the rigid body dynamics of the model. The structure and parameters of this model are to be adjusted to replicate as close as possible the experimentally obtained open loop frequency response and time response data, once it is available in Phase II. For the simulation results presented, each of these parameters was selected to have an adverse effect on the closed loop response. The selection therefore represents a hypothetical worst-case situation.

The Phase I effort demonstrated successful adaptive control of the simulated wind tunnel test article employing flow devices for control. This was accomplished in simulation using *only an approximate model of the synthetic jet actuator* derived from experience and existing data, *demonstrating adaptation* to both unmodeled unsteady aerodynamic effects, and changes in angle of attack and airspeed, and *clearly establishing feasibility*. Alternate flow control actuation schemes were also developed in phase I, highlighting a key advantage of the nonlinear adaptive control approach - that it can be applied to a variety of flow control devices, not just synthetic jets, and to any combination thereof. *Also note that while it was shown that it is not necessary to employ local flow measurements to implement this approach, it is anticipated that the NN may be able to employ such measurements to advantage.* The experience gained from the simulations during Phase I was used for concomitant design of the experimental hardware and wind tunnel model for Phase II of the proposed project.

A phase II program is recommended in which the team will further develop the proposed methods, and demonstrate real-time adaptive output feedback control of the dynamics of the test

article in the low speed tunnel, with rapid transition at the conclusion of phase II to a free flight demonstration.

References

- [1] SMITH, B. L. and GLEZER, A., "Vectoring and Small-Scale Motions Effected in Free Shear Flows using Synthetic Jet Actuators," AIAA paper 97-021, 335th Aerospace Sciences Meeting, 1997.
- [2] SMITH, B. L. and GLEZER, A., "The Formation and Evolution of Synthetic Jets," *Phys. Fluids*, 10, 2281-2297, 1998.
- [3] HONOHAN, A. M., AMITAY, M. and GLEZER, A., "Aerodynamic Control using Synthetic Jets", AIAA Paper 2000-2401, Fluids 2000 Conference, Denver, CO, 2000.
- [4] GLEZER, A., AMITAY, M., and HONOHAN, A. M., "Aspects of Low- and High-Frequency Aerodynamic Flow Control," AIAA Paper 2003-0533, 2003 (accepted for publication in *AIAA Journal*).
- [5] HOVAKIMYAN, N., YANG, B. J., and CALISE, A. J., *An adaptive output feedback control methodology for non-minimum phase systems*. In Proceedings of Conference on Decision and Control, December 2002, Las Vegas, Nevada.
- [6] CALISE, A. J., YANG, B. J., and CRAIG, J. I., *An augmenting adaptive approach to control of flexible systems*. In Proceedings of AIAA Guidance, Navigation, and Control Conference, August 2002, Monterey, California.
- [7] IDAN, M., CALISE, A. J., KUTAY, A. T., and PAREKH, D. E., *Adaptive neural network based approach for active flow control*. In ASME Fluids Engineering Division Summer Meeting, number FEDSM2001-18281, New Orleans, Louisiana, May 2001.
- [8] CALISE, A. J., EL-SHIRBINY, H., KIM N., KUTAY, A. T., *An adaptive guidance approach for spinning projectiles*. In Proceedings of AIAA Guidance, Navigation, and Control Conference, August 2004, Providence, Rhode Island.

Appendix A

Design of an Alternate Wind Tunnel Test Apparatus

The original test concept involved a wind tunnel model comprised of a nominally 2-D airfoil instrumented with flow control actuators and having two degrees of freedom namely rotation about a spanwise axis through its center of gravity and vertical translation (see Progress Report 1). As noted in Section 2, the design was expanded in phase I to include a light-weight glider-like platform that can be used for autonomous loitering. The mission will use low-power flow control devices to allow for maneuver without the activation of conventional, servo-powered control surfaces thereby maximizing mission duration and reducing the required payload (e.g., batteries and servo hardware).

In this Appendix we present an alternate means for flow control actuation - a novel, flow-control approach that is specifically designed for low-speed applications and is based on bleeding air from the pressure (lower) side of the aerodynamic surfaces (the wing and the tail) to the suction (upper) surface. This "controlled porosity" can be implemented using piezoelectrically driven light weight louvers as shown below.

The global view of the test apparatus remains as shown in Figure 1 of Section 2. The vertical guide rail also remains as presented in Section 2. The conventional servo-actuated trailing edge control surface is also unchanged.

The proposed demonstration vehicle is designed to fly at relatively low speeds for loitering missions. In this alternate design, flow control is to be accomplished by bleeding air flow from the pressure side of the aerodynamic surfaces (wing and tail) to the suction side. Controlled porosity will be accomplished using piezoelectrically-operated louvers that will be integrated into the skin on the suction side as shown in Figure A.1. In the inactive (normal) position, these louvers are designed to bleed continuously. Control will be achieved by proportional displacement of the louvers between completely open and closed positions thereby regulating the bleed rate and the derived control of lift and pitching moment. Piezoelectric actuators are selected because of their exceedingly low power consumption (zero in the rest position), simplicity, and agility. These attributes also enable substantial redundancy and therefore overall improved reliability. The fluid mechanics and aerodynamic effects of actuation at low Reynolds numbers will be investigated in detail during the early stages of the proposed Phase II research in the Georgia Tech wind tunnel. In conjunction with the actuator configurations shown here, approaches for controlled dynamic trapping, accumulation and shedding of vorticity concentrations will also be investigated.

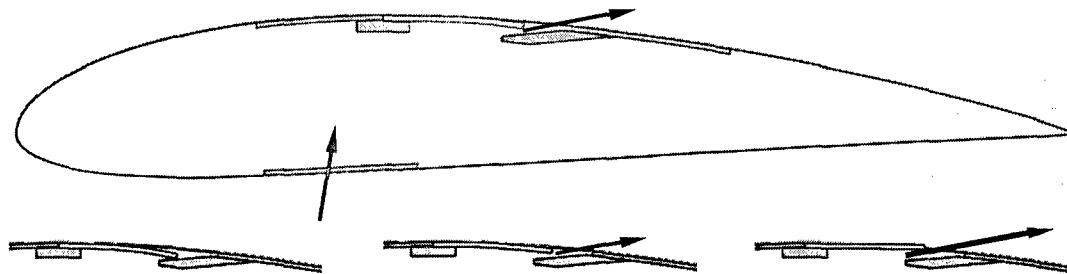


Figure A.1. Flow control actuators (bottom row from left to right: fully closed, unactuated, and fully open positions).